ACS OMEGA

http://pubs.acs.org/journal/acsodf

Article

Biological Preparation of Chitosan-Loaded Silver Nanoparticles: Study of Methylene Blue Adsorption as Well as Antibacterial Properties under Light

Wensheng Ren, Qian Tang,* Hongyu Cao, Lihao Wang, and Xuefang Zheng*

Cite This: *ACS Omega* 2023, 8, 22998−23007

Read Online

ACCESS | Metrics & More | Article Recommendations

ABSTRACT: Human beings have made significant progress in the medical field since antibiotics were widely used. However, the consequences caused by antibiotics abuse have gradually shown their negative effects. Antibacterial photodynamic therapy (aPDT) has the ability to resist drug-resistant bacteria without antibiotics, and as it is increasingly recognized that nanoparticles can effectively solve the deficiency problem of singlet oxygen produced by photosensitizers, the application performance and scope of aPDT are gradually being expanded. In this study, we used a biological template method to reduce Ag^+ to silver atoms in situ with bovine serum albumin (BSA) rich in various functional groups in a 50 °C water bath. The aggregation of nanomaterials was inhibited by the protein's multistage structure so that the formed nanomaterials have good dispersion and stability. It is unexpected that we used chitosan microspheres (CMs) loaded with silver nanoparticles (AgNPs) to adsorb methylene blue (MB), which is both a pollutant and photosensitive substance. The Langmuir adsorption isothermal curve was used to fit the adsorption capacity. The exceptional multi-bond angle chelating forceps of chitosan make it have a powerful physical adsorption capacity, and dehydrogenated functional groups of proteins with negative charge can also bond to positively charged MB to form a certain amount of ionic bonds. Compared with single bacteriostatic materials, the bacteriostatic capacity of the composite materials adsorbing MB under light was significantly improved. This composite material not only has a strong inhibitory effect on Gram-negative bacteria but also has a good inhibitory effect on the growth of Gram-positive bacteria poorly affected by conventional bacteriostatic agents. In conclusion, the CMs loaded with MB and AgNPs have some possible applications in the purification or treatment of wastewater in the future.

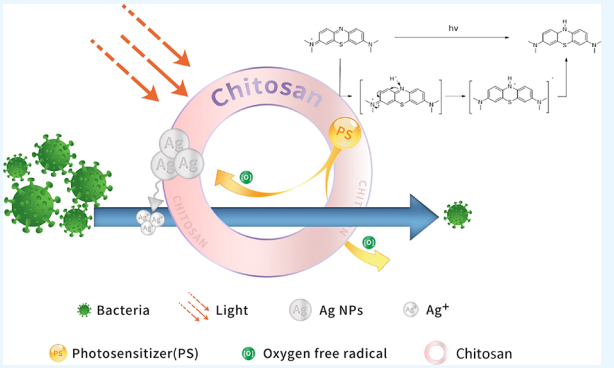

INTRODUCTION

In recent decades, antibiotics and antibacterial medications have made remarkable progress in the treatment of a variety of diseases, which has greatly promoted the development of medical field.[1,2] However, the recent increase in the prevalence of antibiotic-resistant strains has become a big headache.[3,4] The continuous evolution of drug-resistant strains will have a great impact on medical field or will render the current medical methods ineffective or weak.[5−10] Under these circumstances, some innovative and effective methods or materials are needed to deal with these diseases caused by drug-resistance bacteria.

Photodynamic therapy (PDT) is a promising therapy;[11−14] under light irradiation, photosensitizers are excited to produce free radicals, and free radicals will produce singlet oxygen in the presence of oxygen. Singlet oxygen has certain cytotoxicity to the target due to its super oxidation.[15] Antibacterial photodynamic therapy (aPDT) is a photodynamic therapy for drug resistant strains, which is used to kill or eliminate pathogens.[16−18] Because of their strong oxidation, they have a certain effect on the cell membrane of bacteria and even changes the physiological activity of bacteria by entering bacteria.[18−20] In the existing research, the key of aPDT is the content of oxygen-free radicals produced by photosensitizers. The insufficient generation of oxygen-free radicals is the main barrier to the wide application of aPDT.

Nanomaterials have been extensively applied in various industries due to their many superior characteristics.[21−28] The combination of metal nanoparticles and biological preparation technology has an extraordinary significance in the medical field, which is green and has better performance.[29−32] Nanomaterials exhibit great bactericidal ability to drug-

Received: March 29, 2023
Accepted: May 18, 2023
Published: June 15, 2023

https://doi.org/10.1021/acsomega.3c02111
ACS Omega 2023, 8, 22998−23007

resistant bacteria by bypassing the traditional bactericidal mode of antibiotics.[33] Ivask's research[34] shows that the physical properties of AgNPs have specific toxicity to *Escherichia coli* (*E. coli*). According to a majority of researchers,[35−37] the antibacterial mechanism is that AgNPs can adhere to cell walls and membranes, damage their structures or components, and cause bacterial eradication. Nanomaterials are powerful tools for humans to kill pathogens by targeting bacterial cell membranes and penetrating bacteria.[38] Nanomaterials loaded with antibiotics have strong bactericidal activity, which can inhibit the formation of the bacterial biological membrane and overcome antibiotic resistance.[39] Gu et al.[40] bonded more than 60 vancomycin antibiotics on gold nanomaterials through Au−S bond. It has been discovered that although individual antibiotics are ineffective against *Escherichia coli* strains, they are effective when the antibiotics have been bound to nanomaterials. In this regard, nanomaterials show great prospects in replacing antibacterial agents and improving the efficacy of antibiotics.[33]

With the further research, it is found that the introduction of nanomaterials in aPDT can compensate for the absence of oxygen-free radical emission.[41] At the same time, it can considerably improve the overall antibacterial performance of the system. On the one hand, nanomaterials can be used as carriers to improve their targeting in the aPDT process. On the other hand, they can also promote the photolysis of photosensitizers, release more singlet oxygen, improve cytotoxicity, and enhance the therapeutic effect of aPDT.[42−45] Chen's results[46] show that silver nanoparticles combined with the photosensitizers will be oxidized to silver ions in the presence of light. Simultaneously, the photosensitizers will release more singlet oxygen, and interactions between photosensitizers and AgNPs can increase the antibacterial effect. In the study of Khoza and Nyokong,[47] the singlet oxygen output of phthalocyanine was increased after the combination of zinc tetra amino phthalocyanine and AgNPs under the same light.

However, the traditional preparation methods of AgNPs require a lot of chemical reagents that could not be recycled, which leads to some waste. In this research, AgNPs were synthesized using a biological template approach after evaluating numerous approaches. BSA as the template stabilizes the AgNPs against aggregation and serves as an anchoring point for the forming AgNPs. AgNPs@BSA created by mixing the BSA and fresh silver ammonia solution was loaded onto chitosan, and they were dipped into the organic dye solution to absorb MB, which is not only an organic dye waste but also a photosensitizer. In this way, the waste methylene blue was adsorbed by AgNPs@BSA/chitosan and was used as a photosensitizer in aPDT to make the composite material play a highly effective antibacterial effect. In comparison to the single material, chitosan-loaded AgNPs and MB will exhibit enhanced antibacterial characteristics. This antibacterial effect is different from that of traditional antibiotics. It will not make bacteria resistant and may also have a certain disinfection and sterilization effect on drug-resistant bacteria.

EXPERIMENTAL SECTION

Materials. Bovine serum albumin (bioanalytically pure), chitosan, silver nitrate, ammonia water, sodium hydroxide, acetic acid, glycerine, methylene blue, and 1,3-diphenylisopropyl furan (analytically pure) were directly purchased; The strains of *Escherichia coli* and *Staphylococcus aureus* are gifts from Colleague Dr. LI in the laboratory. The water used in the experiment was deionized water.

Synthesis of AgNPs. The method reported in the literature was modified. 48 AgNPs were prepared by using BSA instead of the traditional reductant sodium borohydride, while converting the silver nitrate solution into silver ammonia solution. $AgNO_3$(0.063 g) was dissolved with a small amount of water. Then, concentrated ammonia water was added; the solution initially appeared turbid but eventually became clear as the concentrated ammonia was added. The final concentration of the silver ammonia solution was 50 mmol/L after it was placed into a 25 mL volumetric flask and filled to constant volume. Following this, 20 mL of the solution was added into a 50 mL beaker. 0.25 g of BSA was dissolved in 25 mL of deionized water and mixed evenly. The prepared BSA and silver ammonia solutions were incubated in water at 50 °C, respectively. Subsequently, they were mixed and incubated in water for another 90 min at 50 °C. The solution that turned yellow green was the AgNPs@BSA that we needed. After allowing to stand for 24 h, AgNPs@BSA turned into an orange yellow solution; then, they were stored at 4 °C.

Synthesis of AgNPs@BSA/Chitosan Materials. 2 g of chitosan powder was added to 100 mL of 3% (v/v) glacial acetic acid solution, which was then thoroughly dissolved in the mixture, and then, 1 mL of glycerine was added, while being stirred. After stirring and dissolving, the solution was allowed to stand until the whole solution was transparent and chitosan material was obtained.

To obtain AgNPs@BSA/chitosan material (1:1), first, 20 mL of chitosan material was combined with 20 mL of the manufactured AgNPs@BSA; then, this mixture was stirred for 30 min.

Preparation of CMs and AgNPs@BSA/CMs. Separately, the chitosan solution and the AgNPs@BSA/chitosan solution were placed into the syringe. Using a microinjection pump, the syringe was squeezed at a speed of 2.5 mm/min to slowly inject the solution into 2.0 mol/L NaOH, while continuously stirred to produce milky white microspheres, and then repeatedly rinsed with deionized water to bring the pH value of the microspheres to neutral. After being submerged in a tiny amount of deionized water, the microspheres were then chilled for 24 h at 4 °C to harden them into milky white CMs and light-yellow AgNPs@BSA/CMs.

Standard Curve of MB. To create a solution with a concentration of 1×10^{-3} mol/L, 0.0030 g of MB was dissolved in 10 mL of deionized water and kept out of the light. Thirty groups of MB solutions with concentration gradients of 1×10^{-6}−1×10^{-3} mol/L were created at this concentration. A solution of 2 mL from each group was added to the cuvette, and its absorption value at 664 nm was detected using a UV−visible spectrometer. Deionized water was used as the blank control.

The standard curve was drawn using concentration (c) as the abscissa and absorbance (A) as the ordinate. The regression equation of A and c as well as the correlation coefficient (r^2) was found by linear fitting the data with the least square method.

Effect of Concentration on MB Adsorption. 2 mL of MB solution was added to a 5 mL centrifuge tube. Each centrifuge tube was then filled with 5 AgNPs@BSA/CMs, each with a consistent particle size and mass of 0.025 g. By using an

https://doi.org/10.1021/acsomega.3c02111
ACS Omega 2023, 8, 22998−23007

Table 1. Factors of Different Experimental Conditions in Bacteriostasis Test

	A				B			
time	1[a]	2[a]	3[a]	4[a]	1[a]	2[a]	3[a]	4[a]
1 (6 h)	A11	A21	A31	A41	B11	B21	B31	B41
2 (12 h)	A12	A22	A32	A42	B12	B22	B32	B42
3 (18 h)	A13	A23	A33	A43	B13	B23	B33	B43
4 (24 h)	A14	A24	A34	A44	B14	B24	B34	B44
5 (30 h)	A15	A25	A35	A45	B15	B25	B35	B45
6 (36 h)	A16	A26	A36	A46	B16	B26	B36	B46
7 (42 h)	A17	A27	A37	A47	B17	B27	B37	B47
8 (48 h)	A18	A28	A38	A48	B18	B28	B38	B48

[a]1 represents 5 CMs, 2 represents 5 MB/CMs, 3 represents 5 AgNPs@BSA/CMs, and 4 represents 5 AgNPs@BSA@MB/CMs.

UV−visible spectrophotometer, the OD_{664} of MB was determined.

The corresponding MB concentration can be obtained through the regression equation of the standard curve. The average of the three results for each group was then used as the experimental data. The adsorption capacity of MB on the medium, q_e (mmol/g), can be calculated using formula (1).

$$q_e = (C_0 - C_e)/m \times V \quad (1)$$

C_0 and C_e were the initial and equilibrium concentrations of MB concentration (mmol/L), respectively. V is the volume of solution (L), and m is the mass of the particles (g).

The material adsorbing MB was AgNPs@BSA@MB/CM, which can be used in the following study.

Characterization. A UV−vis spectrophotometer (V-560, Jasco Company in Japan) was used to measure the absorption spectra of the solution of silver nitrate, BSA, and AgNPs@BSA, respectively. With 280 nm as the excitation wavelength, the fluorescence emission spectra of the aforementioned materials were measured using a fluorescence spectrometer (FP-6500, Jasco Company in Japan). The size and potential of materials were detected using dynamic light scattering and a zeta potentiometer (NanoBrook 90plus zeta). The morphology of AgNPs@BSA@MB/CMs was studied using SEM (ZEISS Gemini 300) and TEM (FEI Tecnai F20). The crystallinity and phase of AgNPs@BSA@MB/CMs were characterized by XRD (Rigaku SmartLab SE).

Bacteriostatic Effect. *E. coli* (group A) and *S. aureus* (group B) stored at −80 °C were inoculated in LB medium at 37 °C for 12 h in a constant temperature shaking chamber. The bacterial solution was adjusted to a fixed value; that is, the OD_{600} of the solution was 0.6 and then stored at 4 °C after 1000 times dilution. 20 μL of bacteria solution of *E. coli* and *S. aureus* was inoculated into the tubes containing 3 mL of LB of groups A and B, respectively. In the experiment, different types of CMs were placed in group A1 and group A2, respectively, and 8 parallel experiments were set up in each group as displayed in Table 1 for detailed classification. Finally, OD_{600} was measured every 6 h until 48 h. There were three parallel tests given to each group. The matching tagged bacterial solution was obtained every 6 h to measure OD_{600}, while the four sets of samples were incubated at 37 °C in a constant temperature oscillation chamber.

Effect of Light on Bacteriostasis of Materials. The experimental procedure mentioned above was repeated. Following preparation, four groups of samples were irradiated for 20 min using a xenon lamp in ice water solution. Four groups of samples were incubated in a constant temperature shaker incubator at 37 °C, and OD_{600} was measured every 6 h.

Effect of Light Time on the Bacteriostatic Effect of Materials. The experimental samples for group A were placed into 9 test tubes, each containing 3 mL of LB liquid culture medium, 20 μL of *E. coli* , and 5 AgNPs@BSA@MB/CMs. *S. aureus* was added to group B in place of *E. coli*. These test tubes were irradiated for 0, 10, 20, 30, 40, 50, 60, 90, and 120 min in the same xenon lamp lighting, respectively (three parallel tests for each group). All samples were incubated in a constant temperature shaker at 37 ° C for 12 h, and their OD_{600} was measured.

Effect of Material Composition on the Antibacterial Effect of Materials. A test tube was filled with 3 mL of growth medium and 20 μL of either *E. coli* or *S. aureus* (groups A or B), which were then labeled with the relevant group numbers. As a control, five CMs were introduced to A1(B1), five MB/CMs were applied to A2(B2), and five AgNPs@BSA/CMs were put to A3(B3). A4(B4) was added to five AgNPs@BSA (1:1) @MB (1×10^{-5})/CMs. A5(B5) was added to five AgNPs@BSA (1:1) @MB (5×10^{-5})/CMs. A6(B6) was added to five AgNPs@BSA (1:1) @MB (1×10^{-4})/CMs. A7(B7) was added to five AgNPs@BSA (1:3) @MB (1×10^{-4})/CMs. A8(B8) was added to five AgNPs@BSA (1:2) @MB (1×10^{-4})/CMs. A9(B9) was added to five AgNPs@BSA (2:1) @MB (1×10^{-4})/CMs. For each group, three parallel tests were run. All samples were exposed to a xenon lamp for 20 min after being incubated for 6 h in a constant temperature shock chamber. Then, 100 μL of each bacterial solution was spread on a solid medium and incubated in an incubator at 37 °C for 24 h. Finally, the number of colonies on the Petri dish was recorded through a colony counter.

Release of Ag^+. Each of ten AgNPs@BSA/CMs and AgNPs@BSA@MB/CMs were placed in 4 mL of deionized water for 24 h, respectively. ICP-OES (Agilent 725ES(OES)) was used to determine the amount of Ag^+ in deionized water. The control was deionized water containing CMs. The next step was to confirm if light affects the release of Ag^+ by a series of contrast experiments in the dark and in the light.

Release of Singlet Oxygen. The singlet oxygen release rate was determined using the modified approach.[49] In the experiment, the probe 1,3-diphenylisophenylpropanefuran (DPBF) was chosen. The fluorescent probe DPBF can sensitively and effectively react with singlet oxygen before converting into 1,2-diphenylbenzene very soon. As a result, the amount of oxygen-free radicals emitted can be inferred indirectly from the decrease in DPBF absorbance. In a dark environment, 20 μL of DPBF at a concentration of 1000 ppm in dimethyl sulfoxide (DMSO) was prepared, and then, it was

https://doi.org/10.1021/acsomega.3c02111
ACS Omega 2023, 8, 22998−23007

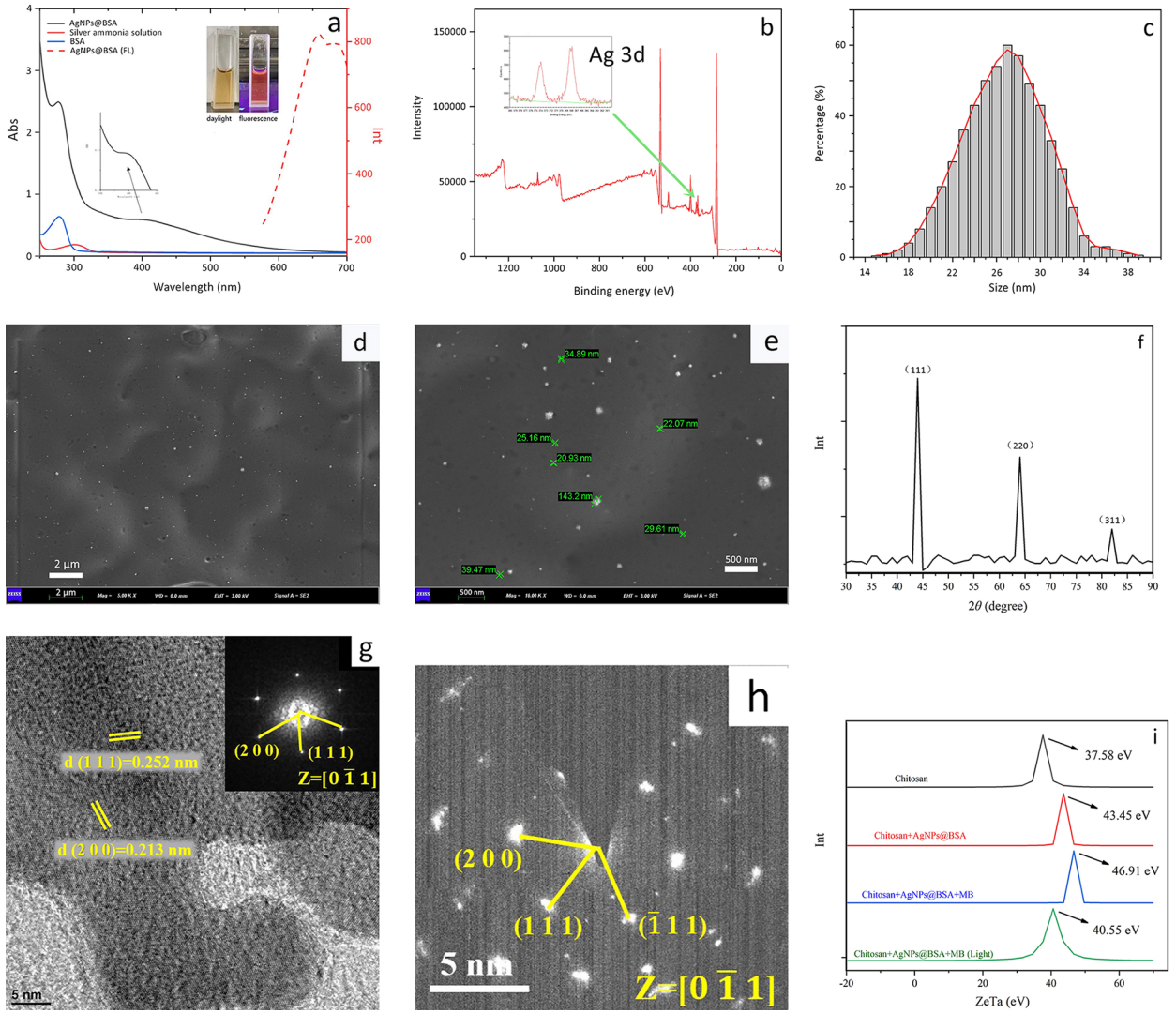

Figure 1. Characterization of the materials of AgNPs@BSA. (a) Ultraviolet spectra of silver nitrate (solid red line), BSA (solid blue line), and AgNPs@BSA (solid black line), and the fluorescence spectra of AgNPs@BSA (dotted red line). The illustration is of AgNPs@BSA under fluorescent lamp (left) and ultraviolet lamp (right). (B) XPS of AgNPs@BSA. Here, the $3d_{3/2}$ and $3d_{5/2}$ peaks of Ag is illustrated. (c) DLS of AgNPs. The scales of SEM of AgNPs@BSA are 2 μm (d) and 500 nm (e) respectively. (f) XRD of AgNPs@BSA. (g) TEM of AgNPs@BSA. (h) SAED of AgNPs@BSA. (i) Potential changes of the MB absorption of CMs and photolysis reaction.

added to the cuvette containing 2 mL of MB solution. In order to rule out the self-degradation of DPBF itself, a blank control group without MB was also created. The absorption spectra were measured after the solution was exposed to a 600 nm xenon lamp for every two minutes. By calculating the decrease of DPBF absorbance over time, the release rate of singlet oxygen produced by MB was determined. When AgNPs were added to MB based on the results of the previous studies, the previous experiment was repeated in order to determine the impact of AgNPs@BSA on the release of singlet oxygen from MB.

RESULTS AND DISCUSSION

Preparation of the AgNPs@BSA. The traditional preparation method of silver nanoparticles is to reduce silver nitrate by using sodium borohydride as the reducing agent and adding a certain capping agent. Gebregeorgis et al.[48] developed a method in which BSA is used to replace the traditional capping agent, so AgNPs are reduced in situ on the multi-level structure of the protein. In this experiment, the method was further modified. Through the use of concentrated ammonia water, silver nitrate is converted to silver ammonia solution, and then, Ag^+ and various functional groups (such as −NH, −OH, and −SH) of BSA are directly reacted[50] in a water bath at 50 °C using the biological template method to form AgNPs without sodium borohydride. The multi-level structure of the protein serves as a barrier to the synthesis of silver nanoparticles, keeping their size within a narrow range and enabling successful dispersion.[51]

Characterization. The AgNPs@BSA solution is yellow when it is just prepared, but after several days of storage, it will turn pale brown, as illustrated in the insets of Figure 1a. In the UV-vis spectra, Ag shows a unique absorption peak at 400 nm as everyone knows. It can be seen from Figure 1a that AgNPs@BSA prepared with bovine serum albumin in this experiment has a very wide absorption band at 300−500 nm and an obvious peak at 400 nm compared with BSA. The fluorescence emission spectra of the prepared material show an obvious peak at 685 nm at the excitation wavelength of 280 nm, as shown in the dotted red line in Figure 1a; the result is

https://doi.org/10.1021/acsomega.3c02111
ACS Omega 2023, 8, 22998−23007

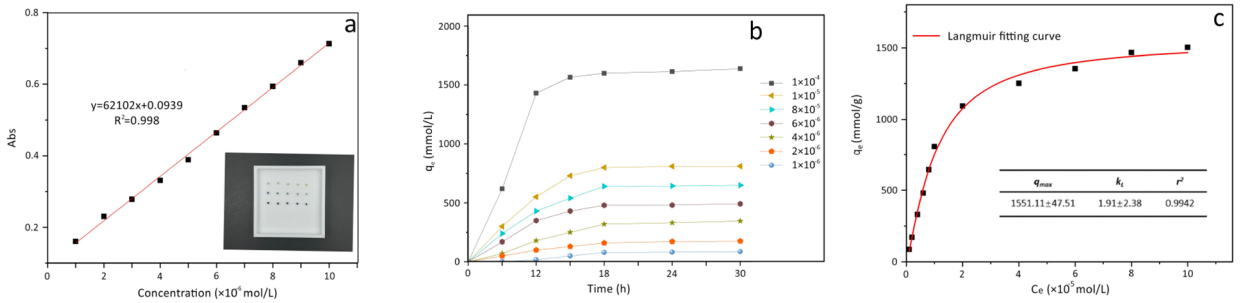

Figure 2. Adsorption of MB by AgNPs@BSA/CMs. (a) Standard curve of methylene blue. The illustration shows the color changes of AgNPs@BSA/CMs adsorbed at different concentrations of MB. (b) Time course of the adsorption capacity (q_e) in different concentrations of methylene blue. (c) Adsorption capacity of microspheres in different concentrations of MB and the fitting of the Langmuir adsorption curve (red line). The illustration shows q_e, k_L, and r^2 of the fitting curve.

consistent with the literature,[52] and the inset of Figure 1a shows the red fluorescence of the material under ultraviolet light.

In addition, the composition of our material was characterized by XPS, as shown in Figure 1b. In the spectrum, two peaks are fitted by Ag, and the binding energy is located at 368 and 375 eV, respectively, which are attributed to the classical peaks of $Ag3d^{3/2}$ and $3d^{5/2}$, respectively.

Figure 1c shows the particle size distribution diagram of the material measured by DLS, from which we can find that the size of the material is concentrated at 28 nm, showing a normal distribution curve.

Figure 1d,e shows the SEM image of the surface of the microspheres loaded with silver nanomaterials. We can clearly observe that a large number of AgNPs was attached to the surface (white dots in the figures). Among these, it can be seen from Figure 1e that most of the sizes are distributed around 25 nm, and the particles size of a small part of materials reaches 143.2 nm, which is consistent with the particle size range (Figure 1c).

Figure 1f shows the XRD pattern of AgNPs@BSA. The crystalline nature of Ag confirmed by XRD spectra. Three main characteristic peaks were observed at 2θ = 44.76 (111), 64.35 (220), and 82.64 (311). These peak positions coincide with those of standard silver. The result was the evidence of the Ag nanomaterials prepared.

To further investigate the crystal structure of AgNPs@BSA, TEM and SAED analyses were carried out. Figure 1g,h shows the results of TEM and SAED, in which the crystal forms of the spots of SAED and FFT (Fast Fourier Transform) both conform to the structure θ of the face-centered cubic crystals.

Through zeta potential, the MB absorption of CMs and photolysis reaction were studied, as Figure 1i. In general, if the absolute value of zeta potential of the material is more than 30, it will have a certain stability. According to the figure, the prepared composite material is stabilized. Chitosan, as a naturally positively charged material, has a potential of 37.58 eV, and when AgNPs@BSA and MB are added, the potential shifts to the right. Although the potential of AgNPs@BSA detected in our previous work is −8 to −10 eV, the potential of chitosan was increased with the addition of AgNPs@BSA and MB. This may be because chitosan is diluted and the overall conductivity increases, resulting in an increase in the overall stability of the material. When we provide the light conditions, MB and AgNPs@BSA react with each other to carry out photolysis consumption, and the potential shifts to the left. However, due to the bonding and adsorption between MB and chitosan, the structure of chitosan was changed, resulting in certain changes in the potential compared with the initial level.

Adsorption of MB by Materials. For polysaccharides, which exist in nature, the chitosan molecules are the only a kind of alkaline polysaccharides. Its special multi-bond angle chelating forceps have a powerful adsorption force and a particular physical adsorption for MB. The substance will also perform chemical adsorption on MB because the protein contains numerous functional groups, which makes the materials have a certain amount of negative electricity due to the release of H^+. In contrast, the N atom of the substituent in MB is positive.[53−55] In order to quantitatively detect the amount of MB adsorbed by the materials, the OD_{664} was first measured in different concentrations of MB to make a standard. We find that the concentration above 1×10^{-4} mol/L of the absorbance value of MB is not available, which do not conform to Lambert−Beer's law, so we choose the MB concentration of 1×10^{-6}−1×10^{-5} mol/L of the absorbance value that is used to draw the standard curve of MB, as shown in Figure 2a. The formula (2) is

$$y = 0.62102x + 0.0939,\ r^2 = 0.9981 \quad (2)$$

Then, we submerged the microspheres in methylene blue solutions of varying concentrations, and by monitoring changes in the methylene blue solution's absorbance value, we were able to calculate the microspheres' adsorption capacities. The color changes of microsphere-adsorbed MB of various concentrations are depicted in Figure 1 illustration. The adsorption concentration C_e of MB was calculated from the standard curve by measuring OD_{664}. Then, the adsorption capacity of AgNPs@BSA/CMs on methylene blue of different concentrations could be calculated by substituting into formula (1), as shown in Figure 2b. It can be seen from Figure 2b that the adsorption capacity increases with the increase of the concentration of MB because the driving force of MB solution overcomes the mass transfer resistance of dye between the aqueous phase and the adsorbent.[54] The Langmuir adsorption isotherm refers to the relationship curve between solute molecular concentration and the adsorbed amount in the adsorption process at a certain temperature, and it is assumed that a single molecule has an active site with uniform binding sites and equivalent energy.[56] According to Langmuir's empirical formula (3):

$$q_e = (q_{max} k_L C_e)/(1 + k_L) \quad (3)$$

q_{max} and k_L represent the maximum adsorption capacity of the solid phase and the energy constant of adsorption heat,

https://doi.org/10.1021/acsomega.3c02111
ACS Omega 2023, 8, 22998−23007

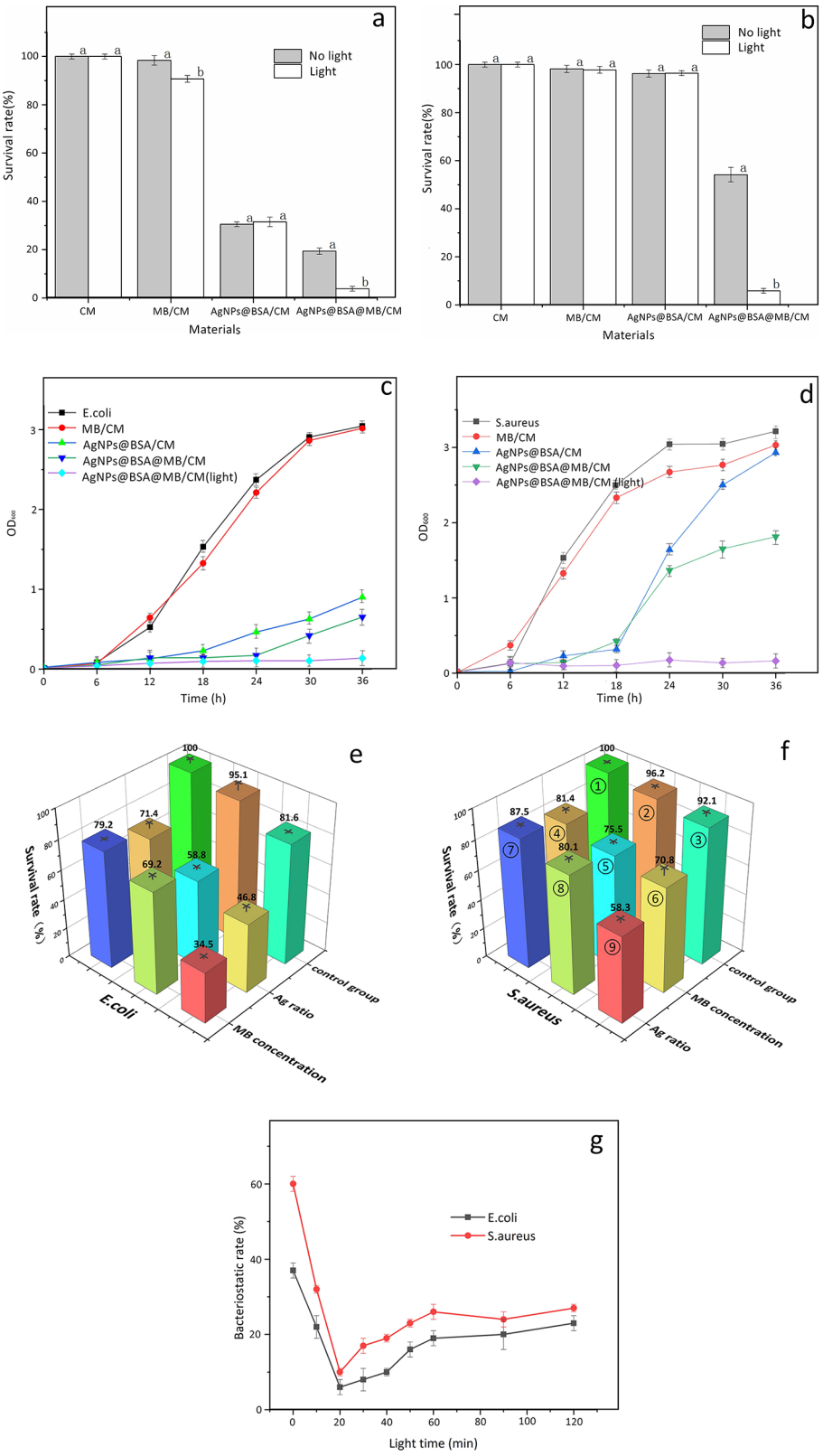

Figure 3. Bacteriostatic effect of AgNPs@BSA@MB/CMs. Inhibition rate of CMs(CM), MB/CMs, AgNPs@BSA/CMs and AgNPs@BSA@MB/CMs against *E. coli* (a) and *S. aureus* (b) with or without light. (^{a,b} means there are significant differences between the two groups ($p < 0.05$) with the same microsphere marked the different superscript letters a and b in accordance with Tukey's test). Growth curves of *E. coli* (c) and *S. aureus* (d) under various material conditions. The bacteriostatic rate of *E. coli* (e) and *S. aureus* (f) by different concentration and ratio of materials. (g) Bacteriostasis rate of microspheres against *E. coli* and *S. aureus* after different light duration.

respectively. The fitted Langmuir diagram is shown in Figure 2c, and the illustrations show the value of Langmuir's correlation parameters k_L, q_{max}, and correlation coefficient r^2. According to q_{max} of microspheres, 1551.11 ± 47.51 mmol/g,

https://doi.org/10.1021/acsomega.3c02111
ACS Omega 2023, 8, 22998−23007

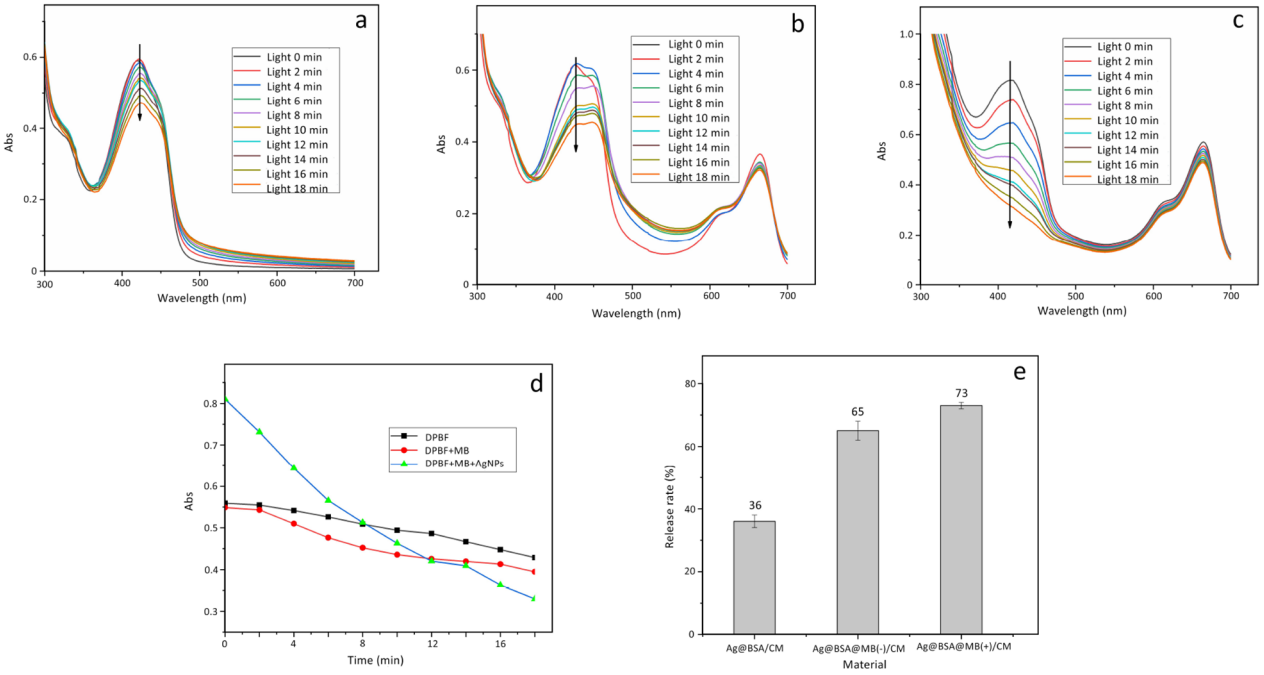

Figure 4. Ultraviolet spectra of DPBF (a), DPBF+MB (b), and DPBF+MB+AgNPs (c) under different illumination times. (d) Absorbance of DPBF, DPBF+MB, and DPBF+MB+AgNPs at 410 nm as a function of time. (e) Ag^+ release rate of AgNPs@BSA/CMs and AgNPs@BSA@MB/CMs; "-" means dark, and "+" means light.

we can know that each microsphere with a mass of 0.025 g prepared can adsorb about 38.77 mmol MB. The r^2 value is 0.9942, which indicates that the measured data fit well with the Langmuir model and indicates that the adsorption process is single molecule adsorption.

Bacteriostatic Effect. *E. coli* and *S. aureus* are used as the representatives of gram-negative bacteria and gram-positive bacteria in the experiment. During the xenon lamp illumination experiment, the material was placed in the ice water mixture to eliminate the influence of high temperature caused by light. Figure 3a,b shows the change of the bacteriostatic rate of different materials under or without light. Through the significance difference analysis of SPSS, neither CMs nor AgNPs@BSA/CMs have any obvious effect on the bacteriostatic action for *E. coli* and *S. aureus* with or without light. In addition, MB/CMs have significant differences on the total antibacterial effect before and after light exposure, but these differences could not be significantly reflected in the antibacterial effect. Hence, these factors were not taken into account in the subsequent experiments, and only the effect of light on the bacteriostatic performance of AgNPs@BSA@MB/CMs was considered.

The growth curve of the bacterial solution is shown in Figure 3c,d. It can be seen from Figure 3c,d that the curve for the first 6 h represents the hysteresis period of bacterial growth. After 6 h, the bacteria entered the logarithmic growth phase. CMs containing the photosensitizer MB do not exhibit excellent antibacterial efficacy because the growth characteristics of the bacterial solution treated with MB/CMs are identical to that of the control group. MB/CMs have a slight effect on *S. aureus*, but they have a noticeable effect on *E. coli*. This may be the result of extremely low concentration of MB adsorbed on chitosan. According to Figure 3c,d, the microspheres containing AgNPs have a poor antibacterial impact on *S. aureus* but a substantial antibacterial effect on *E. coli*. This is due to the fact that the thickness of the Gram negative bacterium's outermost peptidoglycan layer is just 7−8 nm, but the size of peptidoglycan in the cell wall of Gram-positive bacteria ranges from 20 to 80 nm.[57] AgNPs and MB have been loaded onto CMs, which improves the materials' overall antibacterial efficacy, and this phenomenon can be seen even in Figure 3a−d. The colony density of the two materials co-loaded on CMs decline after 36 h, or when they reach a stable period, regardless of whether they are Gram-positive or Gram-negative bacteria, as can be seen from the growth curve of the bacterial solution. After illumination, we can find that for *E. coli*, the bacteriostatic efficiency of AgNPs and MB co-loaded on CMs is 87% higher than that of AgNPs alone and 96% higher than that of MB alone. For *S. aureus*, the bacteriostatic efficiency of the CMs loaded with AgNPs and MB together is 94% higher than that loaded with AgNPs alone and 95% higher than that loaded with MB alone. Therefore, the CMs loaded with the photosensitizer MB and silver nanoparticles developed by us show a strong bacteriostatic effect against Gram-negative bacteria and a weak bacteriostatic effect against Gram-positive bacteria without irradiation. The inhibition rate and long-term inhibition time of AgNPs@BSA@MB/CMs to Gram-negative and Gram-positive bacteria can be improved by light conditions.

We have investigated the amount of photosensitizer and how the ratio of silver nano to chitosan affect the antibacterial impact in order to further enhance the material's overall antibacterial performance. The concentration of the photosensitizer shall be greater than 1×10^{-6} mol/L to reach the minimum excitation concentration of the photosensitizer. There is not an upper limit of concentration for MB, but the concentration that reaches the maximum adsorption capacity of the microsphere limited the number of microspheres in this experiment to 1×10^{-4} mol/L. In the experiment, we counted the colonies cultured on the solid culture medium through the

https://doi.org/10.1021/acsomega.3c02111
ACS Omega 2023, 8, 22998−23007

colony counter and calculated the bacteriostatic rate as shown Figure 3e,f. From the graph, it can be seen that the antibacterial effect is enhanced with the increase of concentration of the photosensitizer. At the same time, to assess the materials' ability of inhibiting bacterial growth, we adjusted the ratio of silver nanoparticles and photosensitizers. The different solubilities of chitosan in acidic and alkaline solutions, as well as the spherical shape produced by surface tension, are responsible for the production of microspheres. The higher proportion of Ag will dilute the concentration of chitosan and lead to the instability of CMs. Therefore, when the content of AgNPs@BSA in the solution is too high, the microspheres will be damaged, the oxidization of microsphere will be slowed down, and the yield of the generated microspheres will be also reduced. Although increasing the proportion of Ag can improve the bacteriostatic rate relatively, it is more practical to increase the yield by slightly reducing the concentration of Ag. In general, it is vital to regulate the proportion of AgNPs and MB in order to enhance the test material's bacteriostatic action. According to the available experimental data, it can be known that the material concentration ratio of AgNPs@BSA(1:1)@MB(1×10^{-4})/CM is the most suitable.

Since light has an impact on the bacteriostatic action of materials, the optimal light time has been determined by adjusting the light time. Figure 3g shows that the material's overall bacteriostatic effect is quite good during the 20−60 min light period. Although the material was kept in a low temperature environment of the ice water mixture during the light time, since the light would produce high temperature, it is preferable to choose a light condition of 20 min in order to prevent the temperature from having an impact on the material.

Bacteriostatic Mechanism. MB is an ionic compound and has three states of MB^+, MB, and MBH. The wide conjugated structure of MB makes it simple to achieve charge transfer and the electron delocalization phenomenon. It is easy to transfer the electron from the N at position 5 to the N of the substituent.[58,59] When illuminated, MB obtains energy, and then is excited, which will produce an intermediate in the excited state, MB. MB in the excited state will cause a free radical reaction to convert molecular oxygen into singlet oxygen. Strong oxidative properties of oxygen-free radicals aid in the transformation of AgNPs into Ag^+ and their release in solution. Because an important reason for the antibacterial property of the material is the generation of oxygen-free radicals, we used DPBF to indirectly count the content of free radicals created throughout the entire lighting process. The photodegradation rate of DPBF alone was extremely slow in the light environment, as illustrated in Figure 4a. The photodegradation rate increases after adding photosensitizer MB because it can over release oxygen-free radicals when exposed to light, as seen in Figure 4b. As shown in Figure 4c, the absorbance of DPBF at 410 nm rapidly reduces after the addition of AgNPs@BSA@MB/CMs, which shows that the system's free radical production increased as a result of the interaction between the materials. The interaction between AgNPs and photosensitizer MB can enhance the release of oxygen-free radicals from the photosensitizer, as seen in Figure 4d.[60]

It can be observed from the ICP-OEC experimental data in Table 2 that the release of Ag^+ in AgNPs@BSA/CM is 36% in their natural form. Under light irradiation, the release of Ag^+ in the solution increased significantly after the adsorption of MB, which reached 73%. This is because the oxygen-free radicals are generated by methylene blue, some of which interact with silver nanoparticles, which then oxidized the silver to form Ag^+ before being released into the solution in the form of ions that have antibacterial properties.

Table 2. Release Rate of Ag^+

	AgNPs@BSA/CM	AgNPs@BSA@MB/CM
the concentration of Ag in the material	441.25 mg/L	441.25 mg/L
the concentration of Ag in the solution	53.20 mg/L	105.14 mg/L
the concentration of Ag in the solution under light	51.81 mg/L	239.47 mg/L

The silver nanoparticles easily connect with bacterial cell membranes and destroy them, subsequently inflicting harm on bacteria and impairing their normal physiological processes, which are their strongest antibacterial quality. In this experiment, BSA with many reduction groups can not only be used as the configuration framework but also as the preparation agent of silver nanomaterials to produce a large number of silver nanoparticles. A particular amount of photosensitizer can be put into the entire chitosan environment. When exposed to light, photosensitizers will react and release a specific number of oxygen-free radicals. The cell membrane of bacteria can be destroyed by oxygen-free radicals due to their powerful oxidation, which results in irreparable harm and prevents bacteria from growing. However, when AgNPs and photosensitizers are in the same environment, the oxygen-free radicals released from the photosensitizers will react with the AgNPs to release more Ag^+ to further destroy the bacterial membrane. Finally, a synergistic bacteriostatic effect is achieved.

In the process of releasing oxygen-free radicals, the increase of the mode of oxygen-free radical release will also promote the increase of the overall release of oxygen-free radicals. As a result, the interaction between them causes the two bacteriostatic materials to have a stronger bacteriostatic effect on gram-positive bacteria than they would have otherwise and a better bacteriostatic effect on gram-negative bacteria. The materials of AgNPs@BSA@MB/CMs also have a good antibacterial impact on bacteria resistant to medication treatments since the antibacterial mechanism of the entire process differs from that of typical antibiotic therapy.

CONCLUSIONS

The green biological template method that used bovine serum albumin (BSA) as the reducing and finishing agents is successfully applied to produce Ag nanoparticles. The combination of Ag nanomaterials and chitosan can adsorb more MB of organic dye. MB's photosensitive quality is also used to give the composite materials superior antibacterial activity when exposed to light. The singlet oxygen generated by the photosensitizer MB has a strong oxidation ability, which can oxidize AgNPs to produce Ag^+, enhance the material's overall antibacterial effectiveness, and cause some degree of bacterial damage. Composite materials offered a new way to enhance the bacteriostatic performance of the materials by light in addition to improving the typical silver nanoparticles' weak bacteriostatic effect on gram-positive bacteria. The compounds discussed in this research will also have some effect against resistant bacteria because the bacteriostatic

https://doi.org/10.1021/acsomega.3c02111
ACS Omega 2023, 8, 22998−23007

mechanism differs from that of conventional antibiotics. Furthermore, the materials created for this article have the potential to both purify and sterilize various water sources and reduce the environmental pollution caused by organic dyes. In future, they might be applied in the cleaning of natural water close to some dye facilities as well as in the treatment of sewage from laboratories.

AUTHOR INFORMATION

Corresponding Authors

Qian Tang − *Liaoning Key Laboratory of Bio-Organic Chemistry and College of Life and healthy, Dalian University, Dalian 116622, China*; Phone: +86 15524852857; Email: tangqian@dlu.edu.cn

Xuefang Zheng − *College of Environmental and Chemical Engineering and Liaoning Key Laboratory of Bio-Organic Chemistry, Dalian University, Dalian 116622, China*; orcid.org/0000-0001-9985-242X; Phone: +86 13941164782; Email: dlxfzheng@126.com

Authors

Wensheng Ren − *College of Environmental and Chemical Engineering, Dalian University, Dalian 116622, China*

Hongyu Cao − *Liaoning Key Laboratory of Bio-Organic Chemistry and College of Life and healthy, Dalian University, Dalian 116622, China*

Lihao Wang − *College of Environmental and Chemical Engineering and Liaoning Key Laboratory of Bio-Organic Chemistry, Dalian University, Dalian 116622, China*

Complete contact information is available at: https://pubs.acs.org/10.1021/acsomega.3c02111

Author Contributions

W.R. contributed to performing the formal analysis and preparing the original data. Q.T. contributed to supervision and review and editing. H.C. and L.W. was involved in formal analysis and validation. X.Z. contributed to supervision and conceptualization.

Notes

The authors declare no competing financial interest.

ACKNOWLEDGMENTS

The authors acknowledge the financial support from the National Natural Science Foundation of China (Nos. 21601025, 21571025, and 21601024), the Scientific Research Projects in Universities of Education Department of Liaoning Province (LJKQZ2021168), the Scientific Research Platform Project of Dalian University (202101ZD01), and the Excellent Youth Team for Scientific Research, Innovation and Entrepreneurship of Dalian University (XQN202004, 2023, and XLJ202005).

REFERENCES

(1) Blahova, J.; Kralikova, K.; St Krcmery, V. Antibiotic resistance. *Cas. Lekaru Ces.* **1999**, *138*, 343−347.

(2) Urban-Chmiel, R.; Marek, A.; Wieczorek, K.; Dec, M.; Stepien-Pysniak, D.; Nowaczek, A.; Osek, J. Antibiotic Resistance in Bacteria-A Review. *Antibiotics* **2022**, *11*, 1079.

(3) Papp, M.; Solymosi, N. Review and Comparison of Antimicrobial Resistance Gene Databases. *Antibiotics* **2022**, *11*, 339.

(4) Nwobodo, D. C.; Ugwu, M. C.; Anie, C. O.; Al-Ouqaili, M. T. S.; Ikem, J. C.; Chigozie, U. V.; Saki, M. Antibiotic resistance: The challenges and some emerging strategies for tackling a global menace. *J. Clin. Lab. Anal.* **2022**, *36*, No. e24655.

(5) Glover, J. S.; Ticer, T. D.; Engevik, M. A. Profiling Antibiotic Resistance in Acinetobacter calcoaceticus. *Antibiotics* **2022**, *11*, 978.

(6) Ferri, G.; Lauteri, C.; Vergara, A. Antibiotic Resistance in the Finfish Aquaculture Industry: A Review. *Antibiotics* **2022**, *11*, 1574.

(7) Patangia, D. V.; Ryan, C. A.; Dempsey, E.; Stanton, C.; Ross, R. P. Vertical transfer of antibiotics and antibiotic resistant strains across the mother/baby axis. *Trends Microbiol.* **2022**, *30*, 47−56.

(8) Lewis, J. S.; Jorgensen, J. H. Inducible clindamycin resistance in staphylococci: Should clinicians and microbiologists be concerned? *Clin. Infect. Dis.* **2005**, *40*, 280−285.

(9) Parra, A.; Ponte, C.; Cenjor, C.; Martinez-Marin, C.; Soriano, F.; Spanish Pneumococcal Infection Study Network. Effect of antibiotic treatment delay on therapeutic outcome of experimental acute otitis media caused by *Streptococcus pneumoniae* strains with different susceptibilities to amoxicillin. *Antimicrob. Agents Chemother.* **2004**, *48*, 860−866.

(10) Ali, J.; Awan, M. O. U.; Akca, G.; Zeb, I.; Amin, B. A. Z.; Ahmad, R.; Shah, M. M.; Nazir, R. Prevalence of diversified antibiotic resistant bacteria within sanitation related facilities of human populated workplaces in Abbottabad. *PLoS One* **2020**, *15*, No. e0233325.

(11) Dang, J. J.; He, H.; Chen, D. L.; Yin, L. C. Manipulating tumor hypoxia toward enhanced photodynamic therapy (PDT). *Biomater. Sci.* **2017**, *5*, 1500−1511.

(12) Li, X.; Lee, S.; Yoon, J. Supramolecular photosensitizers rejuvenate photodynamic therapy. *Chem. Soc. Rev.* **2018**, *47*, 1174−1188.

(13) Monro, S.; Colon, K. L.; Yin, H. M.; Roque, J.; Konda, P.; Gujar, S.; Thummel, R. P.; Lilge, L.; Cameron, C. G.; McFarland, S. A. Transition Metal Complexes and Photodynamic Therapy from a Tumor-Centered Approach: Challenges, Opportunities, and Highlights from the Development of TLD1433. *Chem. Rev.* **2019**, *119*, 797−828.

(14) Chu, E. S. M.; Lo, O. W.; Wu, R. W. K.; Yow, C. M. N. Investigation of the two chlorin-e6 based photosensitizers mediated Photodynamic Therapy (PDT) in human lymphocytes. *Ann. Oncol.* **2021**, *32*, S344.

(15) Usuda, J.; Kato, H.; Okunaka, T.; Furukawa, K.; Tsutsui, H.; Yamada, K.; Suga, Y.; Honda, H.; Nagatsuka, Y.; Ohira, T.; Tsuboi, M.; Hirano, T. Photodynamic therapy (PDT) for lung cancers. *J. Thorac. Oncol.* **2006**, *1*, 489−493.

(16) Amos-Tautua, B. M.; Songca, S. P.; Oluwafemi, O. S. Application of Porphyrins in Antibacterial Photodynamic Therapy. *Molecules* **2019**, *24*, 2456.

(17) Dormoy, J.; Vuillemin, M. O.; Rossi, S.; Boivin, J. M.; Guillet, J. Perceptions of Antibiotic Use and Resistance: Are Antibiotics the Dentists' Anxiolytics? *Antibiotics* **2021**, *10*, 735.

(18) Wu, S. M.; Xu, C.; Zhu, Y. W.; Zheng, L.; Zhang, L. D.; Hu, Y.; Yu, B. R.; Wang, Y. G.; Xu, F. J. Biofilm-Sensitive Photodynamic Nanoparticles for Enhanced Penetration and Antibacterial Efficiency. *Adv. Funct. Mater.* **2021**, *31*, No. 2103591.

(19) Sun, J. Y.; Chen, X.; Mo, S. D.; Zhang, Z.; Guo, D. G.; Li, Y. H.; Liu, L. Recent Advances of Bismuth Halide Based Nanomaterials for Photocatalytic Antibacterial and Photodynamic Therapy. *Adv. Mater. Interfaces* **2022**, *9*, No. 2200704.

(20) Manivasagan, P.; Joe, A.; Han, H. W.; Thambi, T.; Selvaraj, M.; Chidambaram, K.; Kim, J.; Jang, E. S. Recent advances in multifunctional nanomaterials for photothermal-enhanced Fenton-based chemodynamic tumor therapy. *Mater. Today Bio* **2022**, *13*, No. 100197.

(21) Yin, Y. D.; Talapin, D. The chemistry of functional nanomaterials. *Chem. Soc. Rev.* **2013**, *42*, 2484−2487.

(22) Smith, B. R.; Gambhir, S. S. Nanomaterials for In Vivo Imaging. *Chem. Rev.* **2017**, *117*, 901−986.

(23) Das, R.; Vecitis, C. D.; Schulze, A.; Cao, B.; Ismail, A. F.; Lu, X. B.; Chen, J. P.; Ramakrishna, S. Recent advances in nanomaterials for

water protection and monitoring. *Chem. Soc. Rev.* **2017**, *46*, 6946−7020.
(24) Yang, G. J.; Zhang, Y. M.; Cai, Y.; Yang, B. G.; Gu, C.; Zhang, S. X. A. Advances in nanomaterials for electrochromic devices. *Chem. Soc. Rev.* **2020**, *49*, 8687−8720.
(25) Pirzada, M.; Altintas, Z. Nanomaterials for virus sensing and tracking. *Chem. Soc. Rev.* **2022**, *51*, 5805−5841.
(26) Xu, S.; An, H.; Dai, J. Application of Nanomaterials in the Field of New Energy Environment and Economic Benefit Analysis. *Adv. Mater. Sci. Eng.* **2022**, *2022*, 1−10.
(27) Long, L.; Jie, F.; Shuang, L.; Wang, X.; Ma, C.; Li, Y. Application and development of nanomaterials in the field of oilfield chemistry. *N. Chem. Mater.* **2013**, *41*, 187−190.
(28) Wang, X. D.; Yao, C. H.; Wang, F.; Li, Z. D. Cellulose-Based Nanomaterials for Energy Applications. *Small* **2017**, *13*, No. 1702240.
(29) Shin, T. H.; Cheon, J. Synergism of Nanomaterials with Physical Stimuli for Biology and Medicine. *Acc. Chem. Res.* **2017**, *50*, 567−572.
(30) Dickson, R. M. Physical Insights from New Nanomaterials in Biology. *J. Phys. Chem. B* **2017**, *121*, 10733−10734.
(31) Satyavolu, N. S. R.; Loh, K. Y.; Tan, L. H.; Lu, Y. Discovery of and Insights into DNA "Codes" for Tunable Morphologies of Metal Nanoparticles. *Small* **2019**, *15*, No. e1900975.
(32) Li, Y. F.; Liang, Q. W.; Zhou, L. Y.; Liu, J. X.; Liu, Y. H. Metal nanoparticles: a platform integrating diagnosis and therapy for rheumatoid arthritis. *J. Nanopart. Res.* **2022**, *24*, 84−102.
(33) He, J.; Hong, M.; Xie, W. Q.; Chen, Z.; Chen, D. M.; Xie, S. Y. Progress and prospects of nanomaterials against resistant bacteria. *J. Controlled Release* **2022**, *351*, 301−323.
(34) Ivask, A.; ElBadawy, A.; Kaweeteerawat, C.; Boren, D.; Fischer, H.; Ji, Z. X.; Chang, C. H.; Liu, R.; Tolaymat, T.; Telesca, D.; Zink, J. I.; Cohen, Y.; Holden, P. A.; Godwin, H. A. Toxicity Mechanisms in Escherichia coli Vary for Silver Nanoparticles and Differ from Ionic Silver. *ACS Nano* **2014**, *8*, 374−386.
(35) Duran, N.; Duran, M.; de Jesus, M. B.; Seabra, A. B.; Favaro, W. J.; Nakazato, G. Silver nanoparticles: A new view on mechanistic aspects on antimicrobial activity. *Nanomed.: Nanotechnol. Biol. Med.* **2016**, *12*, 789−799.
(36) Franci, G.; Falanga, A.; Galdiero, S.; Palomba, L.; Rai, M.; Morelli, G.; Galdiero, M. Silver nanoparticles as potential antibacterial agents. *Molecules* **2015**, *20*, 8856−8874.
(37) Tang, S. H.; Zheng, J. Antibacterial Activity of Silver Nanoparticles: Structural Effects. *Adv. Healthcare Mater.* **2018**, *7*, No. e1701503.
(38) Munir, M. U.; Ahmad, M. M. Nanomaterials Aiming to Tackle Antibiotic-Resistant Bacteria. *Pharmaceutics* **2022**, *14*, 582.
(39) Thambirajoo, M.; Maarof, M.; Lokanathan, Y.; Katas, H.; Ghazalli, N. F.; Tabata, Y.; Fauzi, M. B. Potential of Nanoparticles Integrated with Antibacterial Properties in Preventing Biofilm and Antibiotic Resistance. *Antibiotics* **2021**, *10*, 1338.
(40) (a) Thambirajoo, M.; Maarof, M.; Lokanathan, Y.; Katas, H.; Ghazalli, N. F.; Tabata, Y.; Fauzi, M. B. Potential of Nanoparticles Integrated with Antibacterial Properties in Preventing Biofilm and Antibiotic Resistance. *Antibiotics* **2021**, *10*, 1338. (b) Gu, H.; Ho, P. L.; Tong, E.; Wang, L.; Xu, B. Presenting Vancomycin on Nanoparticles to Enhance Antimicrobial Activities. *Nano Lett.* **2003**, *3*, 1261−1263.
(41) Li, W. T. Nanotechnology-Based Strategies to Enhance the Efficacy of Photodynamic Therapy for Cancers. *Curr. Drug Metab.* **2009**, *10*, 851−860.
(42) Magalhaes, J. A.; Fernandes, A. U.; Junqueira, H. C.; Nunes, B. C.; Cursino, T. A. F.; Formaggio, D. M. D.; Baptista, M. S.; Tada, D. B. Bimetallic nanoparticles enhance photoactivity of conjugated photosensitizer. *Nanotechnology* **2020**, *31*, No. 095102.
(43) Tian, S. C.; He, J. L.; Lyu, D.; Li, S.; Xu, Q. H. Aggregation enhanced photoactivity of photosensitizer conjugated metal nanoparticles for multimodal imaging and synergistic phototherapy below skin tolerance threshold. *Nano Today* **2022**, *45*, No. 101534.
(44) Liu, J.; Yin, Y. R.; Yang, L. X.; Lu, B. H.; Yang, Z. Y.; Wang, W. D.; Li, R. Nucleus-Targeted Photosensitizer Nanoparticles for Photothermal and Photodynamic Therapy of Breast Carcinoma. *Int. J. Nanomed.* **2021**, *16*, 1473−1485.
(45) Miele, D.; Sorrenti, M.; Catenacci, L.; Minzioni, P.; Marrubini, G.; Amendola, V.; Maestri, M.; Giunchedi, P.; Bonferoni, M. C. Association of Indocyanine Green with Chitosan Oleate Coated PLGA Nanoparticles for Photodynamic Therapy. *Pharmaceutics* **2022**, *14*, 1740.
(46) Chen, J.; Yang, L.; Chen, J.; Liu, W.; Zhang, D.; Xu, P.; Dai, T.; Shang, L.; Yang, Y.; Tang, S.; Zhang, Y.; Lin, H.; Chen, Z.; Huang, M. Composite of silver nanoparticles and photosensitizer leads to mutual enhancement of antimicrobial efficacy and promotes wound healing. *Chem. Eng. J.* **2019**, *374*, 1373−1381.
(47) Khoza, P.; Nyokong, T. Photocatalytic behavior of zinc tetraamino phthalocyanine-silver nanoparticles immobilized on chitosan beads. *J. Mol. Catal. A: Chem.* **2015**, *399*, 25−32.
(48) Gebregeorgis, A.; Bhan, C.; Wilson, O.; Raghavan, D. Characterization of Silver/Bovine Serum Albumin (Ag/BSA) nanoparticles structure: Morphological, compositional, and interaction studies. *J. Colloid Interface Sci.* **2013**, *389*, 31−41.
(49) Ping, J. T.; Peng, H. S.; Duan, W. B.; You, F. T.; Song, M.; Wang, Y. Q. Synthesis and optimization of ZnPc-loaded biocompatible nanoparticles for efficient photodynamic therapy. *J. Mater. Chem. B* **2016**, *4*, 4482−4489.
(50) Mathew, A.; Sajanlal, P. R.; Pradeep, T. A fifteen atom silver cluster confined in bovine serum albumin. *J. Mater. Chem.* **2011**, *21*, 11205−11212.
(51) Sun, N. R.; Wu, H.; Shen, X. Z.; Deng, C. H. Nanomaterials in Proteomics. *Adv. Funct. Mater.* **2019**, *29*, No. 1900253.
(52) Mathew, A.; Sajanlal, P. R.; Pradeep, T. Selective visual detection of TNT at the sub-zeptomole level. *Angew. Chem., Int. Ed.* **2012**, *51*, 9596−9600.
(53) Chen, X.; He, L. Microwave Irradiation Assisted Preparation of Chitosan Composite Microsphere for Dye Adsorption. *Int. J. Polym. Sci.* **2017**, *2017*, 1−8.
(54) Jyothi, M. S.; Angadi, V. J.; Kanakalakshmi, T. V.; Padaki, M.; Geetha, B. R.; Soontarapa, K. Magnetic Nanoparticles Impregnated, Cross-Linked, Porous Chitosan Microspheres for Efficient Adsorption of Methylene Blue from Pharmaceutical Waste Water. *J. Polym. Environ.* **2019**, *27*, 2408−2418.
(55) Wan, X.; Rong, Z.; Zhu, K.; Wu, Y. Chitosan-based dual network composite hydrogel for efficient adsorption of methylene blue dye. *Int. J. Biol. Macromol.* **2022**, *222*, 725−735.
(56) Langmuir, I. The constitution and fundamental properties of solids and liquids. *J. Franklin Inst.* **1917**, *183*, 102−105.
(57) Kim, J. S.; Kuk, E.; Yu, K. N.; Kim, J. H.; Park, S. J.; Lee, H. J.; Kim, S. H.; Park, Y. K.; Park, Y. H.; Hwang, C. Y.; Kim, Y. K.; Lee, Y. S.; Jeong, D. H.; Cho, M. H. Antimicrobial effects of silver nanoparticles. *Nanomed.: Nanotechnol. Biol. Med.* **2007**, *3*, 95−101.
(58) Impert, O.; Katafias, A.; Kita, P.; Mills, A.; Pietkiewicz-Graczyk, A.; Wrzeszcz, G. Kinetics and mechanism of a fast leuco-Methylene Blue oxidation by copper(ii)−halide species in acidic aqueous media. *Dalton Trans.* **2003**, 348−353.
(59) Grishin, D. F.; Lizyakina, O. S.; Vaganova, L. B.; Kaltenberg, A. A.; Grishin, I. D. Radical polymerization of methyl methacrylate in the presence of methylene blue and organobromides under visible light irradiation. *Iran. Polym. J.* **2021**, *30*, 1117−1126.
(60) Mahajan, P. G.; Dige, N. C.; Vanjare, B. D.; Eo, S. H.; Seo, S. Y.; Kim, S. J.; Hong, S. K.; Choi, C. S.; Lee, K. H. A potential mediator for photodynamic therapy based on silver nanoparticles functionalized with porphyrin. *J. Photochem. Photobiol., A* **2019**, *377*, 26−35.

https://doi.org/10.1021/acsomega.3c02111
ACS Omega 2023, 8, 22998−23007